Neutron scattering studies of the cooperative paramagnet pyrochlore $Tb_2Ti_2O_7$

J. S. Gardner,* B. D. Gaulin, A. J. Berlinsky, and P. Waldron
Department of Physics and Astronomy, Canadian Institute for Advanced Research, McMaster University, Hamilton, Ontario, Canada L8S 4M1

S. R. Dunsiger
Department of Physics and Astronomy, University of British Columbia, Vancouver, British Columbia, Canada V6T 1Z1

N. P. Raju† and J. E. Greedan
Brockhouse Institute for Materials Research, McMaster University, Hamilton, Ontario, Canada L8S 4M1
(Received 21 February 2001; published 21 November 2001)

We have carried out extensive neutron-scattering studies on the pyrochlore antiferromagnet $Tb_2Ti_2O_7$ in both polycrystalline and single-crystal form. This insulating material belongs to a family of rare-earth titanate pyrochlores, $R_2Ti_2O_7$, whose magnetic rare-earth ions reside on a network of corner sharing tetrahedra. Such a local geometry is known to give rise to geometrical frustration in the presence of antiferromagnetic interactions. Earlier studies have shown $Tb_2Ti_2O_7$ to be an Ising system with large moments constrained to point along local [1, 1, 1] directions; that is, into and out of the tetrahedra. It displays a cooperative paramagnetic or spin liquid state at low temperatures, with neither long-range Néel order nor spin glass ordering at temperatures as low as 0.07 K. Our elastic neutron-scattering measurements show that very short-range correlations develop below ~100 K. At 4 K a checkerboard pattern of diffuse magnetic scattering within the $[h,h,l]$ plane in reciprocal space is observed, consistent with spin correlations over near neighbors only. Inelastic scattering measurements on both powder and single-crystal samples show three bands of magnetic excitations. At temperatures above ~20 K, these bands are dispersionless, but at low temperature an appreciable softening in the lowest band of excitations occurs at those wave vectors which characterize the development of the very short-range magnetic order, qualitatively consistent with theoretical expectations derived from the single-mode approximation.

DOI: 10.1103/PhysRevB.64.224416 PACS number(s): 75.25.+z

I. INTRODUCTION

Materials containing antiferromagnetically coupled magnetic moments which reside on geometrical units, such as triangles and tetrahedra, that inhibit the formation of a collinear ordered state, often display phenomena known broadly as geometrical frustration.[1] The best-known example occurs for the two-dimensional triangular net and unidirectional, classical, antiferromagnetically-coupled magnetic moments.[2] In such a system, any two moments can align in a spin-up, spin-down arrangement, but the third cannot satisfy both its nearest neighbors simultaneously. In three dimensions with a tetrahedral coordination, the situation is similar with at least two antiferromagnetic (AF) ''bonds'' frustrated at any one time. The ground state of such systems can have a very large spin degeneracy, as it is only constrained by the condition that the vector sum of the spins on a frustrated building block (the triangle or tetrahedron) is zero. Such combinations of antiferromagnetism and geometries based on triangles and tetrahedra are in fact common in nature. Antiferromagnetism is more common than ferromagnetism, and many close-packed crystal structures are based on triangles.

The oxide pyrochlore family, with chemical composition $A_2B_2O_7$, crystallizes into a face-centered-cubic structure with eight formula units per conventional unit cell.[3] The A site is occupied by a trivalent rare-earth ion with eightfold oxygen coordination, while the B site is occupied by a tetravalent transition-metal ion with sixfold oxygen coordination. The sublattice of each of the two metal ions form infinite, interpenetrating, networks of corner-sharing tetrahedra, as shown in Fig. 1.

The literature on this problem goes back to Anderson's classic theoretical treatment of the problem in 1956,[4] and experimental studies have been carried out for more than 15 years. The last decade has seen much attention paid to this area, and substantial experimental and theoretical progress has been made.[1,5–9] It is now clear that classical Heisenberg spins coupled with near-neighbor AF interactions on such a lattice show no transition to long-range Néel order at any temperature,[10,11] while numerical calculations of quantum-mechanical $S=\frac{1}{2}$ moments are suggestive of the same result.[12] These low-temperature states have been referred to as either ''collective paramagnets'' or ''spin liquids'' depending on whether one is referring to classical or quantum-mechanical states, respectively. Such states are quite distinct from those pertaining to the antiferromagnetic, two-dimensional kagomé lattice, a network of corner-sharing triangles, for which an order-by-disorder, spin nematic order occurs at low temperatures.[13]

Many experimental studies have recently been carried out on pyrochlore and related systems.[5–9,14–27] Many of these have revealed classic spin-glass behavior at low temperatures, as characterized, for example, by history dependent and nonlinear susceptibilities. These include $Y_2Mo_2O_7$,[5,6] $Tb_2Mo_2O_7$,[7] and $Y_2Mn_2O_7$,[8] as well as the disordered pyrochlore $CsNiCrF_6$,[9] the disordered kagomé, or pyrochlore-

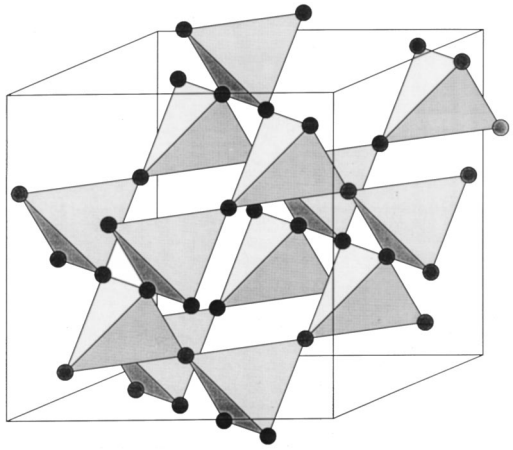

FIG. 1. The pyrochlore lattice. The *A* and *B* atom sublattices for cubic pyrochlores of the chemical composition $A_2B_2O_7$ each, independently, reside on such a network of corner-sharing tetrahedra.

slab, system $SrCr_{9p}Ga_{12-9p}O_{19}$ (Refs. 28–31) and the garnet $Gd_3Ga_5O_{12}$.[32] In oxide pyrochlores, this is a surprising result, as it is generally assumed that a spin-glass ground state requires chemical or bond disorder in addition to competing (or frustrated) interactions.[33] All diffraction studies to date on oxide pyrochlore systems have found them to be periodic, chemically ordered compounds to within the sensitivity of such measurements (roughly 1% for oxygen nonstoichiometry). Recent x-ray-absorption fine-structures measurements on $Y_2Mo_2O_7$ suggested that subtle bond disorder may be present.[18]

The *B* site of the cubic spinels with composition AB_2O_4 also resides on a network of corner-sharing tetrahedra. If this site carries a magnetic moment which is antiferromagnetically coupled, similarly interesting behavior is expected. A recent study of $ZnCr_2O_4$ (Ref. 27) reports on a lattice instability and a local spin resonance at low temperatures, driven by the frustrated magnetic interactions.

Although the two *A* and *B* metal ion sublattices in the pyrochlore structure are identical, the surrounding oxygen ions are different. The *A* atom has eightfold coordination forming a distorted cube of oxygen neighbors. The six oxygen atoms surrounding the *B* atoms form regular octahedrons. The *B*-O distances are all equal and the *B*-O-*B* angle is between 130° and 135° for most pyrochlores. The network surrounding the *A* atom is more complicated. The *A* atoms are in the center of a hexagon of oxygens with the two remaining oxygen atoms, labeled O', above and below this hexagonal plane. The O' atoms are considerably closer to the *A* site than are the six equatorial oxygens and form a quasi-one-dimensional network of zig-zag chains with angles of approximately 109.5° and 180°.

With these differences in mind, and the wide variety of different magnetic species that can occupy the *A* and/or *B* sites, it is not surprising that many physical properties differ from pyrochlore to pyrochlore. Transport studies on pyrochlore compounds showed that the electrical properties are strongly dependent on the atomic radius of the *A* atom. In general for a given *B* atom, as the atomic radius of *A* decreases, the electrical properties of the compound become more metallic. Bulk magnetic properties are varied even among the insulating or semiconducting members of this family, where, with a relatively open structure, only near neighbor magnetic exchange interactions should be relevant. In addition to the spin glass ground states found in $Y_2Mo_2O_7$,[5,6,18,19] $Tb_2Mo_2O_7$,[7] and $Y_2Mn_2O_7$,[8] insulating compounds such as $Er_2Ti_2O_7$ (Ref. 20) display a Néel-ordered ground state, and a singlet, nonmagnetic ground state has been shown to exist in $Tm_2Ti_2O_7$.[21]

This paper focuses on one of the three materials known for which no transition of any kind is observed at low temperatures, potentially consistent with a ''cooperative paramagnetic'' or ''spin liquid'' ground state. Extensive measurements on polycrystalline $Tb_2Ti_2O_7$ (Ref. 22) showed that the system remains in a paramagnetic state to temperatures as low as 0.07 K, despite developing short-range antiferromagnetic correlations as high as 50 K. Measurements on other such systems, $Ho_2Ti_2O_7$ (Ref. 23) and $Dy_2Ti_2O_7$,[24] have been interpreted as evidence of a ''spin ice'' ground state. This state arises most naturally in a classical system with ferromagnetic interactions and strong single ion anisotropy, which then give rise to a disordered ground state. Recent calculations[34] showed that the spin ice ground state is more robust, and that it can exist at low temperatures even in the presence of weak antiferromagnetic exchange, coupled with long-range dipolar interactions.

In this paper we report detailed neutron-scattering studies of $Tb_2Ti_2O_7$ in both single-crystal and polycrystalline forms at temperatures down to 2 K. These measurements significantly extend earlier bulk and neutron measurements on polycrystalline samples,[22] and will allow for a meaningful comparison to theoretical calculations of the magnetic structure factor in the ''cooperative paramagnetic'' ground state. These measurements also complement and extend earlier reports on single crystals.[14,15]

$Tb_2Ti_2O_7$ is an insulator which crystallizes in the cubic, face-centered space group $Fd\bar{3}m$, with a lattice parameter $a=10.15(1)$ Å, at 300 K. At high temperatures the Tb^{3+} ions on the *A* site possess almost the full magnetic moment expected for the free $^7F_6$ Tb^{3+} ion ($9.6\mu_B$), as determined by Curie-Weiss fits to the high-temperature susceptibility. The Ti^{4+} ion, like the O^{2-} ion, is diamagnetic and plays no role in the magnetic nature of this system. Measurements of susceptibility and heat capacity in both $Tb_2Ti_2O_7$ and $(Tb_{1-x}Y_x)_2Ti_2O_7$, as well as neutron spectroscopic measurements of crystalline electric field (CEF) levels in polycrystalline $Tb_2Ti_2O_7$ are fully consistent with CEF calculations which show the ground and first excited states of Tb^{3+} in this environment both to be doublets, separated by roughly 18 K.[16] Both these doublets display very anisotropic *g* tensors with the principal eigenvalues directed along [111] directions. The ground-state moment is large, estimated to be $\sim 5\mu_B$, while the contribution to the Curie-Weiss constant from exchange interactions is $\Theta_{CW}^{ex} \sim -13$ K, antiferromagnetic. Therefore, the Tb moments residing on the corner-sharing tetrahedra lattice in $Tb_2Ti_2O_7$ should be well described by classical, Ising spins constrained to point along local [111] directions (that is, directly into and out of the

local tetrahedra) and these moments interact with each other via near-neighbor antiferromagnetic exchange interactions and longer range magnetic dipole interactions.[16]

II. EXPERIMENTAL DETAILS

Polycrystalline samples of $Tb_2Ti_2O_7$ were prepared by firing stoichiometric amounts of Tb_4O_7 and TiO_2 at 1350° for several days with intermittent grindings to ensure a complete reaction. Large, high-quality, single crystals of $Tb_2Ti_2O_7$ were subsequently grown by the floating zone method under a controlled atmosphere in an optical image furnace, using the polycrystalline material in the single-crystal growth. Several single crystals, approximately 3–5 mm in diameter and up to 20 mm in length, were grown from a small seed crystal in an overpressure of oxygen. Details of this crystal growth were described elsewhere.[14] The phase purity, room-temperature lattice parameters and crystal structure of the polycrystalline and single crystals were confirmed by x-ray diffraction. Susceptibility measurements on both the polycrystalline and single-crystal samples were carried out between 350 and 0.5 K, to confirm earlier muon spin relaxation and specific-heat results[16,22] that $Tb_2Ti_2O_7$ remains in a paramagnetic state down to at least 0.5 K.

The neutron-scattering experiments on polycrystalline samples employed a 20-g powder sample placed in a sealed, thin walled aluminum can with a helium exchange gas to provide thermal contact. The single crystal ($\sim$1 cc) sample was mounted on an aluminum pin and wrapped in aluminum foil to improve the thermal stability of the entire sample. The sample was then mounted in either a helium cryostat or a closed-cycle refrigerator to achieve the desired temperature range.

The polycrystalline diffraction studies were carried out on the DUALSPEC C2 high resolution powder diffractometer at the NRU reactor at the Chalk River Laboratories, with an incident neutron wavelength of 2.37 Å, and a pyrolitic graphite (PG) filter in the incident beam to remove higher order contamination. The 80° detector bank of this diffractometer was moved between two positions in order to obtain data from 3° to 115° in scattering angle. Data were collected for 6 h at several temperatures between 100 and 2 K and at each detector position. Inelastic neutron-scattering experiments were performed on the C5 triple axis spectrometer (TAS) at Chalk River, as well as on the Quasi-elastic spectrometer, (QENS) at the Intense Pulsed Neutron Source (IPNS), Argonne National Laboratory. The TAS measurements were performed in constant scattered energy mode with $E'/h = 3.52$ THz and a PG filter in the scattered beam [resulting in low energy resolution of $\sim$0.20 THz full width of half maximum (FWHM)], as well as with $E'/h = 1.2$ THz and a cooled Be filter in the scattered beam (resulting in a high-energy resolution $\sim$0.09 THz (FWHM). The high-energy resolution time-of-flight experiments on QENS used a larger 50-g polycrystalline sample. QENS is an inverse-geometry spectrometer that accepts a white beam from the cold methane moderator at the IPNS. Bragg reflections from an array of graphite crystals select 15.1 THz neutrons in the scattered beam. These two features result in an energy resolution at the Bragg position of $\sim$0.02 THz. By changing the detector positions it is possible to cover a Q range of $0.5 < Q < 2.5\,\text{Å}^{-1}$.

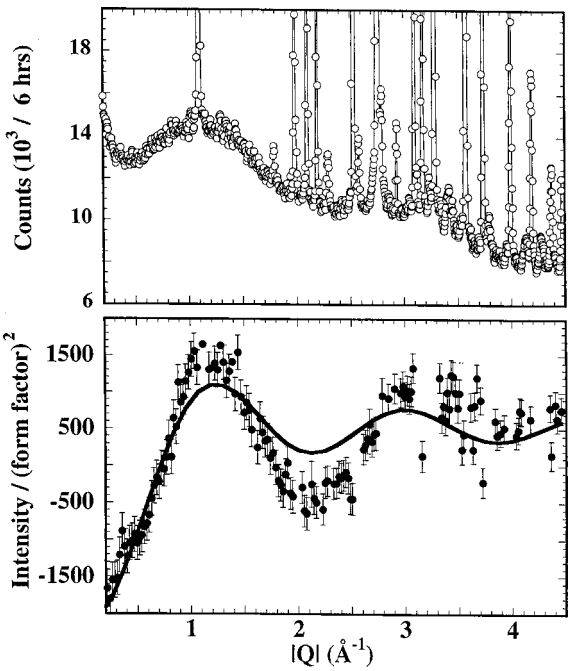

FIG. 2. Top panel: A neutron powder diffraction pattern from $Tb_2Ti_2O_7$ at 2.5 K is shown. Bottom panel: The difference between diffraction patterns taken at 2.5 and 100 K, corrected for the Tb^{3+} magnetic form factor, is shown. The solid line is a fit to the net scattering expected from spins correlated over a single near-neighbor distance in a powder, as described in the text by Eq. (1).

III. NEUTRON SCATTERING FROM POLYCRYSTALLINE SAMPLES

Neutron powder diffraction data from $Tb_2Ti_2O_7$ at 2.5 K is shown in the top panel of Fig. 2. One clearly sees two broad, liquidlike, distributions of scattering centered at roughly 1.2 and 3 Å^{-1}, on which is superimposed a large number of sharp diffraction features originating from the crystalline lattice. The sharp powder Bragg peaks due to the lattice are characteristic of resolution-limited diffraction features, and it is clear, even in this ''raw'' data, that the broad diffraction features are many times resolution width, and consequently arise due to very short-range spin correlations.

The bottom panel of Fig. 2 shows the same low-temperature data set collected at 2.5 K, as shown in the top panel, but with a 100-K data set subtracted from it. Measurements of the temperature dependence of the diffuse scattering, to be discussed below, show that this scattering continues to evolve with temperature, at temperatures as high as 100 K. Consequently, this relatively high temperature data set was employed as a background. The resulting net scattering shows a diffuse, temperature-dependent signal which we identify as magnetic in origin, peaked up near $|\mathbf{Q}_{\text{max}}| \sim 1.2$ and 3.2 Å^{-1}, as the raw data suggested, but now with the considerable nonmagnetic background removed. It is clear that scattering in the forward direction, near $|\mathbf{Q}| \sim 0\ \text{Å}^{-1}$, is

depleted at low temperatures compared to high temperatures, indicating the absence of ferromagnetic correlations. The magnetic structure factor resulting from the subtraction between the two data sets is roughly consistent with an expression used to model the scattering from powders where short-range, isotropic spin correlations exist out to the first few coordination shells of neighbors. This expression[35] is

$$I(Q) \sim \Sigma_{i,j} \langle S_i S_j \rangle \frac{\sin(Q r_{i,j})}{Q r_{i,j}}, \tag{1}$$

which simplifies to

$$I(Q) \sim \frac{\sin(Q r_{i,j})}{Q r_{i,j}} \tag{2}$$

if spins are correlated over nearest neighbors, and consequently only one value of $r_{i,j}$ (the distance between spins at sites i and j) is employed.

This expression, multiplied by the magnetic form factor appropriate to the Tb^{3+} ion,[36] has been fit to the net intensity shown in the bottom panel of Fig. 2, and the result is the solid line in the figure. While the fit does not provide a quantitative account of the diffuse magnetic structure factor, it does place the peaks and valleys at the correct wave vectors, and indicates that, whatever spin correlations are present, they must be of very short range, extending out over near neighbors only.

Inelastic neutron-scattering measurements, with both relatively high- and low-energy resolutions, were also carried out on the powder sample, and a representative low-energy resolution, triple-axis scan at 12 K is shown in the top panel of Fig. 3. In this plot, excitations are evident at ~2.53, 3.50, and 3.90 THz. The latter two are difficult to resolve at this low-resolution configuration. The excitations at ~2.53 and 3.50 THz are identified as magnetic in origin, and the 3.90-THz excitation as an optical phonon, on the basis of their $|\mathbf{Q}|$ dependence. Closer examination of the low-frequency regime of this scan indicates a low-energy band of excitations near ~0.38 THz, which requires a higher-energy resolution to properly resolve. This low-energy excitation is also identified as being magnetic in origin, again due to its $|\mathbf{Q}|$ dependence.

These measurements, performed on a powder sample, reveal excitations which are well defined in energy, implying that the excitations must be relatively dispersionless, as is expected of crystalline electric field excitations. Close examination of the energy-$|\mathbf{Q}|$ relation for these excitations, obtained by fitting inelastic scans as a function of $|\mathbf{Q}|$, bears this out. Such representative inelastic scans, focusing on the two lowest-energy bands of magnetic excitations, are shown in the bottom panel of Fig. 3. The resulting dispersion relationships for each of the three bands of magnetic excitations are shown in Fig. 4, at both relatively low temperature, ($T = 12$ K) and at a higher temperature ($T = 30$ K).

As can be seen in Fig. 4, above ~25 K (roughly the energy of the lowest-energy band of magnetic excitations) all three bands of magnetic excitations are dispersionless, consistent with crystal-field excitations. Indeed, these powder measurements motivated calculations of single-ion properties

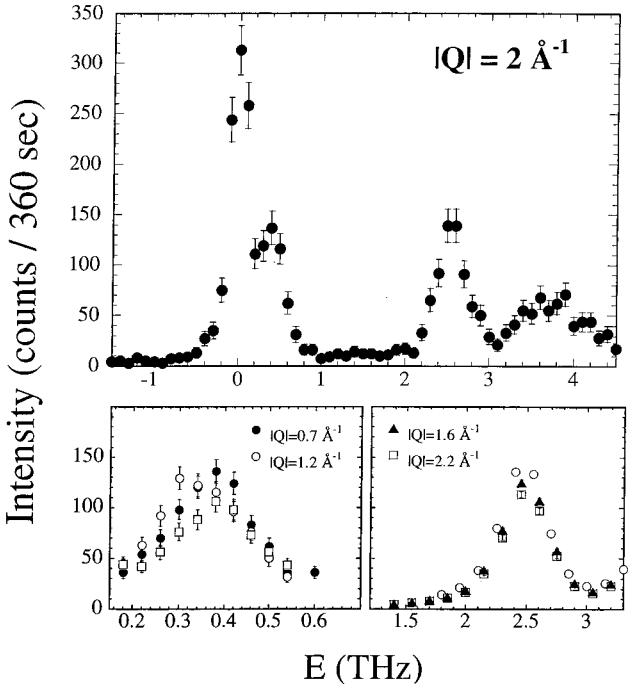

FIG. 3. Top panel: A representative constant $|\mathbf{Q}|$ scan from the powder sample at 12 K showing modes at ~0.36, 2.53, and 3.50 THz. The scattering near 3.5 THz in this plot shows both a magnetic excitation and an optical phonon. Bottom panels: the $|\mathbf{Q}|$ dependence of the two lowest-lying magnetic excitations are shown for the powder sample, again at 12 K.

of Tb^{3+} in the *A*-site environment of the pyrochlore structure appropriate to $Tb_2Ti_2O_7$. A level scheme for the $^7F_6$ ion with $J = 6$ has been determined in which the ground state and first excited states are both doublets, with two higher-energy singlet excited states as shown in Fig. 5.[16] These low-lying states are then well separated in energy from the other crystal-field states. The ground-state doublet is made up primarily of J^z eigenstates $|\pm 4\rangle$ and $|\pm 1\rangle$, and the first excited doublet of eigenstates $|\pm 5\rangle$and $|\pm 2\rangle$. One of the other two singlets corresponds exclusively to $|\pm 6\rangle$ and $|\pm 3\rangle$, while the remaining singlet corresponds to $|\pm 6\rangle$, $|\pm 3\rangle$, and $|0\rangle$. The ground state is connected to all of these low-lying excited states by $\langle A|S^+|0\rangle$ dipole matrix elements, and hence all of these transitions are expected to be visible with neutron spectroscopy.

An interesting feature of these magnetic dispersion relations is that the lowest-energy band *alone* develops an easily measurable dispersion as the temperature is lowered below ~25 K, that is, below the temperature for which the low lying mode would be thermally populated. This dispersion corresponds to a dip in the energy of the excitations at the wave vector which characterizes the very short-range order which the material displays at low temperatures. This is clearly seen in Fig. 4, where a minimum in the dispersion relation occurs at $|\mathbf{Q}| \sim 1.2$ Å^{-1}, and the dispersion relation appears headed toward a second dip as the wave vector comes close to one corresponding to the second minimum in $S(Q)$, ~3 Å^{-1} (measurements at high-energy resolution and

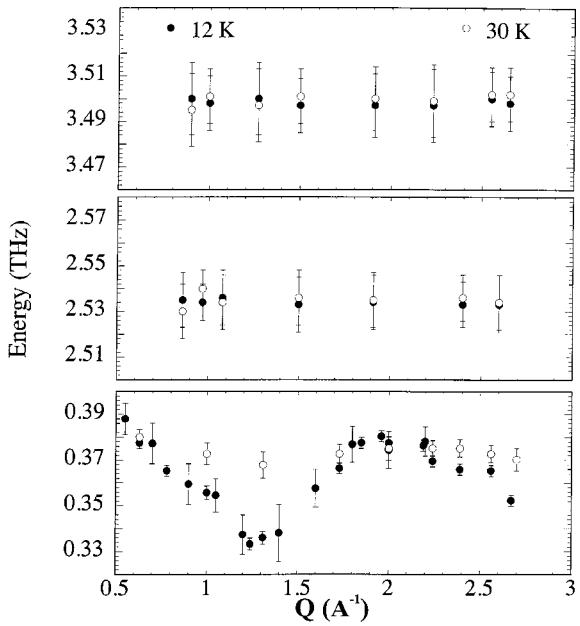

FIG. 4. The dispersion relation of the three lowest-lying magnetic excitations in the polycrystalline sample, at both 12 K (solid symbols) and 30 K (open symbols). Data from both the high-energy resolution triple axis as well as from time-of-flight measurements are presented. Note that only the lowest energy branch displays dispersion below ~20 K, with a partial softening at the wave vector, $|\mathbf{Q}| \sim 1.2$ Å^{-1}, which characterizes the short-range order in the powder sample (see Fig. 2).

relatively high $|\mathbf{Q}|$ are kinematically restricted; consequently our high-resolution inelastic scattering data do not extend to higher $|\mathbf{Q}|$).

Figure 4 shows the dispersion for the three bands of magnetic excitations on the same energy scale, and it is clear that the dispersion which develops at low temperature for the lowest energy band is not present for the higher two. It is not at all clear why this should be the case. The band of excitations near 0.38 THz corresponds to a doublet-doublet transition with the CEF scheme described above, while the two dispersionless bands at ~2.53 and 3.50 THz correspond to doublet-singlet transitions.

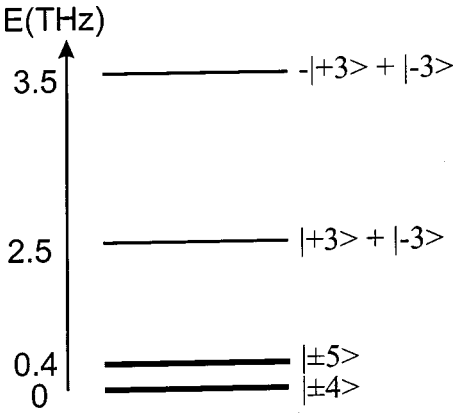

FIG. 5. Energy-level scheme and approximate eigenvectors (see Ref. 16 for the precise eigenvectors) for the lowest-energy multiplet corresponding to Tb^{3+} in a crystalline environment appropriate to $Tb_2Ti_2O_7$. This scheme is based, in part, on the measurements shown in Fig. 4.

IV. NEUTRON SCATTERING FROM SINGLE-CRYSTAL SAMPLES

The availability of the large single-crystal samples of $Tb_2Ti_2O_7$ allow a more detailed examination of both the static and dynamic magnetic behaviors of this material. Measurements of both $S(\mathbf{Q})$ and $S(\mathbf{Q},\hbar\omega)$ can be made, with directional dependencies on $\mathbf{Q}$ revealed directly, as opposed to being averaged out, as occurs in measurements on polycrystalline samples.

Measurements of the magnetic $S(\mathbf{Q})$ from the single-crystal sample of $Tb_2Ti_2O_7$ are shown in the upper panel of Fig. 6. This color contour map of the scattering is made up from the difference between two energy-integrated scans at 9 and 100 K, performed in the (h,h,l) scattering plane. For a cubic system, such a scattering plane is most often employed, as it contains three high-symmetry directions: $(0,0,l)$, $(h,h,0)$, and (h,h,h). As can be seen, the diffuse scattering is clearly anisotropic, roughly made up of a checkerboard pattern of interconnected squares of scattering which extends across entire Brillouin zones. It is now clear why the simple theoretical description, based on an isotropic, liquid-like structure factor for powders [Eq. (2)], failed to adequately describe the diffuse scattering from the polycrystalline samples—the scattering is not isotropic.

The temperature dependence of this energy-integrated diffuse scattering is shown in Fig. 7, where the diffuse scattering intensity at $\mathbf{Q}=(0,0,2.25)$, near the strongest maximum in $S(\mathbf{Q})$, is shown. While the scattering decreases with increasing temperature, most rapidly below ~20 K, a gradual decrease in scattering continues to temperatures as high as ~100 K. It is for this reason that the 100-K scattering data set was employed as the ''background'' for the determination of the magnetic diffuse scattering shown in the upper panel of Fig. 6.

The ~20-K energy scale is manifest repeatedly in our measurements on $Tb_2Ti_2O_7$. The dispersion in the lowest-energy excitation appears only below ~20 K, the average energy of the lowest-energy mode is ~20 K, the temperature dependence in $1/T_1$ as measured in μSR experiments exhibits a plateau at ~20 K; and the temperature dependence of the diffuse magnetic scattering changes slope in a pronounced manner at ~20 K.

Representative constant-$\mathbf{Q}$, inelastic scattering scans as a function of temperature (top panel) and wave vector (bottom panel) are shown in Fig. 8. These data were taken on the single-crystal sample, along the $(0,0,l)$ direction in reciprocal space. The bottom panel explicitly shows the dispersion in the low-lying magnetic excitation at low temperatures, with a minimum in the dispersion relation at the wave vector which characterizes the peak in $S(\mathbf{Q})$ (at $l=2$ in this direction). The top panel shows a neutron group at the minimum of the dispersion relation, as a function of temperature. Taken together, these two panels show the development of the minimum in $E(\mathbf{Q})$ as the temperature is lowered below ~20 K.

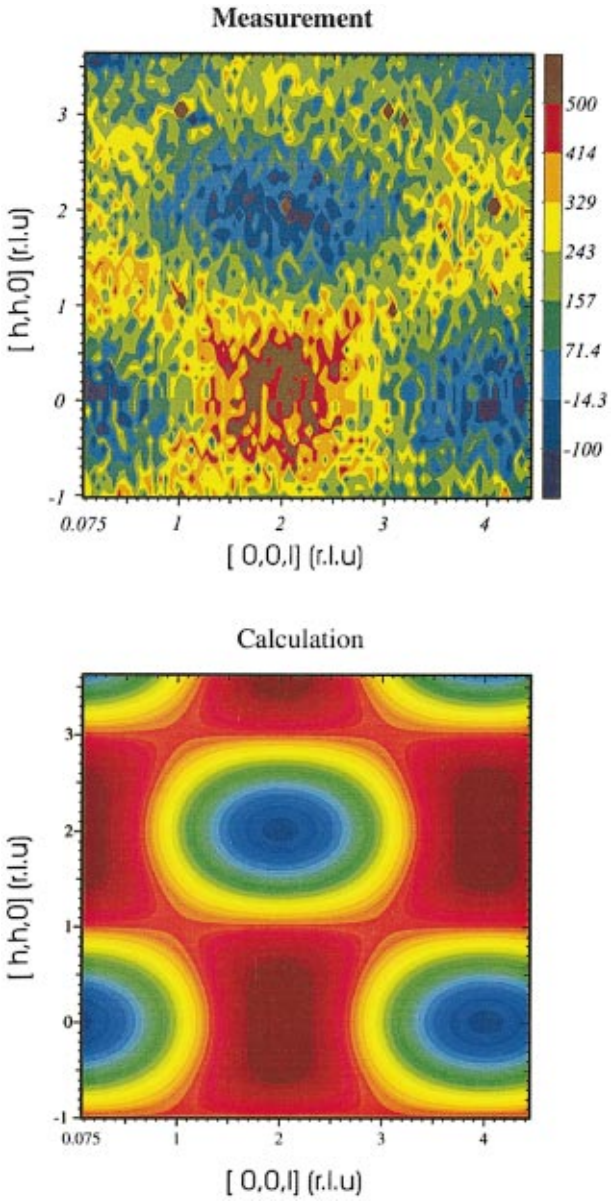

FIG. 6. (Color) Upper panel: A color contour plot of the measured diffuse scattering in the single-crystal sample within the (h,h,l) plane at 9 K is shown. A high-temperature ($T=100$ K) background has been subtracted, so as to isolate the magnetic correlations. Bottom panel: The form of $S(\mathbf{Q})$ calculated on the basis of near-neighbor correlations alone on the pyrochlore lattice [Eq. (3)] is shown. This form differs from Eq. (2), which assumes isotropic near-neighbor spin correlations, and well describes the checkerboard pattern of magnetic scattering within the (h,h,l) plane in reciprocal space, as observed experimentally (see upper panel). The intensity scale in the calculation (lower panel) has been chosen to match that of the experiment (upper panel).

Relatively high counting statistic, energy-integrated, line scans in reciprocal space were performed along the three high-symmetry directions at both 4.2 and 100 K. Their difference, again multiplied by a magnetic form factor appropriate to Tb^{3+}, is plotted in the three panels of Fig. 9. The axis and labels for these $S(\mathbf{Q})$ data are on the left side of the figure. Also plotted on the same figure is the dispersion relation for the lowest-energy band of magnetic excitations at 4.2 K, as determined from constant-**Q** scans of the form shown in Fig. 8. The axis and labels appropriate to these dispersion relations are on the right side of Fig. 9. In all three symmetry directions, different $E(\mathbf{Q})$ dependencies are observed, mirroring the anisotropic nature of $S(\mathbf{Q})$. That is for

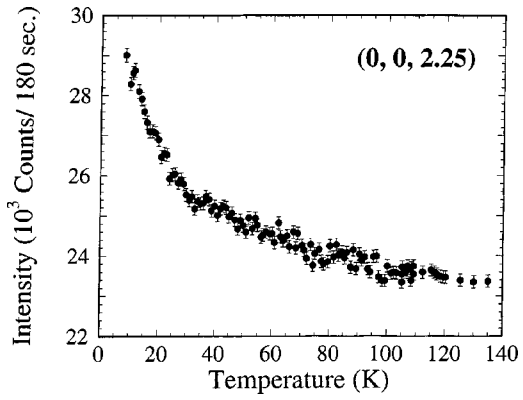

FIG. 7. The temperature dependence of the diffuse scattering from the single-crystal sample at (0,0,2.25) is shown. Note that it develops strong growth with decreasing temperature below 20 K, but continues to evolve with temperature at temperatures as high as 100 K.

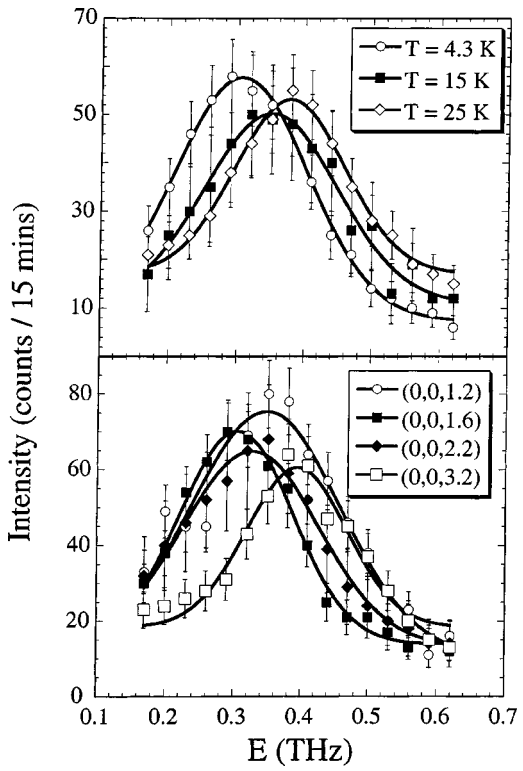

FIG. 8. Constant **Q** scans from the single-crystal sample, revealing the temperature and **Q** dependence of the low-lying magnetic excitation entered at ~0.38 THz, is shown. The top panel shows how this mode softens with decreasing temperature close to $\mathbf{Q}_{\max}$. The **Q** dependence at 4.3 K, for wave vectors along $(0,0,l)$, is shown in the bottom panel. The lines are a guide to the eye.

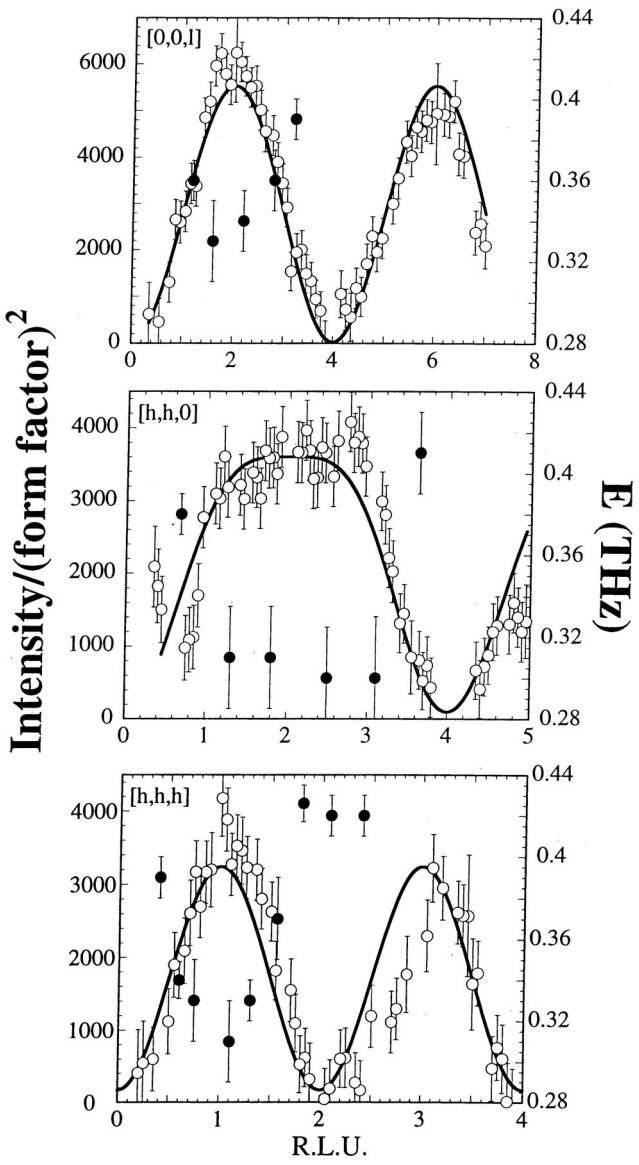

FIG. 9. The open symbols show data from line scans in reciprocal space performed on a single crystal, for the three high-symmetry directions: from top to bottom, $(0,0,l)$, $(h,h,0)$, and (h,h,h). The solid lines are fits of a theoretical expression describing minimal near-neighbor antiferromagnetic spin correlations on the pyrochlore lattice [Eq. (3)]. The label and scale for this intensity data are on the left side of the panels. The filled symbols show the dispersion relation for the lowest-lying branch of magnetic excitations at $T=4.2$ K. Note that in all directions, the minima in the dispersion relations occur at wavevectors for which $S(\mathbf{Q})$ is a maximum.

all $\mathbf{Q}$, the minimum in the dispersion relation, $E(\mathbf{Q})$ clearly corresponds to the maximum in $S(\mathbf{Q})$.

V. DISCUSSION

The color contour map of the measured $S(\mathbf{Q})$ in the upper panel of Fig. 6 clearly shows diffuse magnetic scattering distributed across entire Brillouin zones, therefore originating from a substructure within a single primitive cell. While this result is similar to the results of theoretical studies of the classical Heisenberg antiferromagnet on a pyrochlore lattice, there are important differences. First, $S(\mathbf{Q})$ calculated using Monte Carlo methods displays a pattern of interconnected triangles, as opposed to the checkerboard, or interconnected square, pattern we observe at 9 K from single-crystal $Tb_2Ti_2O_7$. This comparison suggests that we are observing spin correlations which are even shorter range than those displayed by the classical cooperative paramagnetic ground state of the Heisenberg antiferromagnet on the pyrochlore lattice.

We have carried out a simple calculation for $S(\mathbf{Q})$ based on near-neighbor spin correlations alone, the least correlated spin system we can imagine. For $\mathbf{Q}=2\pi(h,k,l)$, the structure factor is given by

$$S(\mathbf{Q})=1+a\{\cos(h\pi/2)\cos(k\pi/2)+\cos(h\pi/2)\cos(l\pi/2)+\cos(k\pi/2)\cos(l\pi/2)\}, \quad (3)$$

where a is the nearest-neighbor spin-spin correlation function, which has the value $-1/3$ at $T=0$.

This expression does indeed produce a checkerboard pattern for $S(\mathbf{Q})$ within the (h,h,l) plane in reciprocal space, as can be seen in the lower panel of Fig. 6, and as experimentally observed in our color contour plot shown in Fig. 6. It is quantitatively compared to the line scans along the three symmetry directions in Fig. 9. As can be appreciated by examination of Eq. (3), the amplitude of $S(\mathbf{Q})$ is the same in all three high-symmetry directions, while the observed scattering amplitude is strongest along $(0,0,l)$. Nonetheless the overall pattern of the calculated $S(\mathbf{Q})$, and the excellent description of the reciprocal-space widths of the diffuse scattering peaks, implies that the spins within $Tb_2Ti_2O_7$ are correlated over near neighbors, that is, within a single tetrahedron only, at these temperatures.

The simple form for the spin correlations given by Eq. (3), does not include the neutron-scattering cross section's sensitivity to components of moment which lie in a plane perpendicular to $\mathbf{Q}$ *only*. This expression [Eq. (3)] differs from Eq. (2), which describes isotropic, liquidlike spin correlations, as the directional dependence of the spin correlations due to the local sixfold coordination of each spin by its near neighbors is now explicitly included in the model.

Earlier neutron-scattering measurements on single-crystal $Tb_2Ti_2O_7$ samples were analyzed and interpreted in terms of a short-range ordered structure in which Tb^{3+} moments were aligned along local $[0,0,l]$, or cube edge, directions, with correlations over a seven spin unit made up of two connected tetrahedra. While such a correlated droplet of ~ 7 spins is consistent with the present measurements (that is, strong correlations present between the spin at the vertex of the two tetrahedra and its near neighbors), the details of the local structure (moment direction) proposed by Kanada *et al.*[15] is not.

It is possible that further cooling to lower temperatures will cause the measured $S(\mathbf{Q})$ to evolve to a form more similar to the interconnected triangle pattern, characteristic of the classical Heisenberg antiferromagnet. However, there are important differences between $Tb_2Ti_2O_7$ and the classical

Heisenberg pyrochlore antiferromagnet. As discussed, all magnetic measurements, and in particular those reported here, which show a gapped magnetic excitation spectrum to frequencies as low 0.18 THz (see Figs. 3 and 8) are consistent with strong Ising anisotropy with the spins pointing into and out of the local tetrahedra at low temperatures. In addition, although the exchange interactions are antiferromagnetic and likely well approximated as near neighbors (due to the open nature of the pyrochlore structure), dipolar interactions are expected to be relatively strong at temperatures below 20 K, due to the large moments present at the Tb^{3+} site.

Somewhat counterintuitively, while antiferromagnetic near-neighbor exchange interactions between isotropic classical spins on the pyrochlore lattice lead to a spin liquid or collective paramagnetic ground state, the presence of strong single ion anisotropy directed along local (*l*,*l*,*l*) directions again favors a Néel-ordered ground state, albeit a noncollinear one in which spins at the vertices of the tetrahedra all point directly into or out of the individual tetrahedra. Such a noncollinear long-range-ordered ground state occurs in FeF_3,[37] whose magnetic Fe ions reside on a pyrochlore lattice. Dipolar interactions are anisotropic, depending as they do on the dot product between the unit vector joining two spins and the vector spin itself. We believe it is the competition between these anisotropic interactions, the antiferromagnetic exchange interactions, and the strong [*l*,*l*,*l*] anisotropy due to CEF effects, which is most likely the mechanism for the absence of a transition to long-range Néel order at temperatures of order 10 K. Indeed, recent theoretical arguments based on Monte Carlo calculations, including these competing interactions, place an upper bound on the temperature at which such Néel ordering can occur.[34]

We naively expected our neutron-scattering measurements of the single-crystal magnetic structure factor to be described by short-range order based on the FeF_3, noncollinear Néel state.[37] This would correspond to expectations for classical, Ising moments, antiferromagnetically coupled to near neighbors, and pointing either into or out of the tetrahedra. However, it is easy to see that such a simple local structure cannot be correct, as the most intense diffuse scattering occurs around (0,0,2). Scattering at this reciprocal space point is due to pairs of spins, π out of phase from each other, across a tetrahedron. However the net spins, added together with a π phase factor for scattering at (0,0,2), are themselves aligned along (0,0,2). Such correlations are not visible to the neutron experiment due to its already mentioned sensitivity to components of moment which lie in a plane *perpendicular* to **Q**. The details of the local structure suggested by Kanada *et al.*[15] have related difficulties. Further, their proposed local structure is based on Tb^{3+} moments aligned along cube edges, which is inconsistent with the CEF calculations appropriate to Tb^{3+} in the $Tb_2Ti_2O_7$ environment.

The dispersion observed at temperatures below 20 K in the low-lying band of magnetic excitations is particularly intriguing. The measurements on single-crystal samples show that the energy, $E(\mathbf{Q})$, of these excitations dips at those wavevectors for which $S(\mathbf{Q})$ is a maximum. This is the same conclusion which was reached on the basis of the polycrystalline data, but we now see that the this relationship holds in single crystals which display an anisotropic $S(\mathbf{Q})$. We also clearly see that a similar dispersion does not develop for the higher-energy bands of excitations at ~2.53 and 3.50 THz, both of which correspond to transitions from the doublet ground state to singlet excited states within the crystal electric-field scheme appropriate to Tb^{3+} in the $Tb_2Ti_2O_7$ environment.

In magnetic systems, an incomplete softening of well-defined excitations has not been observed in other geometrically frustrated magnets, or chemically disordered spin glasses. However, such a behavior has been observed in the amorphous ferromagnet Co_4P.[38] A related behavior was also observed in praseodymium-based intermetallics,[39] wherein both the ground state and first excited state of Pr in isolation in this environment are singlets. Similar effects also occur in the acoustic-phonon spectrum associated with materials near a martenitic structural phase transition.[40] It is not clear whether useful analogies to any of these systems can be made.

The observed behavior of the dispersion of the low-lying magnetic mode is most reminiscent of the roton minimum in the single-particle excitation spectrum of liquid ^{4}He, wherein the energy of the excitations dip at those wave vectors characteristic of the very short-range translational order in liquid ^{4}He. An elegant explanation of this behavior in liquid ^{4}He was provided by Feynmann,[41] who used the single-mode approximation (SMA) to calculate the qualitative features of the entire phonon spectrum in liquid ^{4}He.

Within this framework, the dispersion relation $E(\mathbf{Q})$ is given by the ratio of the oscillator strength to the structure factor $S(\mathbf{Q})$, both of which are properties of the static equilibrium correlations, and are calculable by, for example, Monte Carlo techniques. In the case of liquid ^{4}He, the oscillator strength goes like Q^2, while the structure factor rises only linearly with Q at small Q. The result is the familiar phonon branch in liquid ^{4}He, going to zero energy at $Q=0$, but displaying the roton minimum in $E(\mathbf{Q})$, at the wave vector for which the structure factor peaks, about 2 Å^{-1} in the case of liquid ^{4}He.

SMA calculations using classical averages for the Heisenberg AF on the pyrochlore lattice have been performed,[42] and indicate that *both* the oscillator strength and the structure factor go as Q^2 at low Q, resulting in a *gapped* excitation spectrum with a minimum in $E(\mathbf{Q})$ at those **Q**'s for which the structure factor is maximum. This theoretical result is qualitatively consistent with the experimental dispersion presented in this paper. While it is important to bear in mind the significant differences between the model employed in the SMA calculation for the pyrochlore AF, and the nature of the Tb moments in $Tb_2Ti_2O_7$, it is encouraging that much of this intriguing phenomena is captured by this relatively simple approach. We hope this work will motivate further studies, both experimental and theoretical, which can fully clarify the nature of these excitations and their dispersion.

VI. CONCLUSIONS

Neutron scattering on both polycrystalline and single-crystal samples of $Tb_2Ti_2O_7$ show the development of very

short-range spin correlations for temperatures below ~20 K. The onset of this diffuse magnetic scattering is surprisingly high, ~100 K. The diffuse magnetic scattering within the (h,h,l) reciprocal-space plane displays a checkerboard, interconnected square pattern which has some similarities to the results of Monte Carlo calculations for $S(\mathbf{Q})$ of the classical Heisenberg antiferromagnet on a pyrochlore lattice. However, the measurements are better described by a simple model in which spins are minimally correlated, that is only to near neighbors on the corner-sharing tetrahedral lattice. A detailed understanding of the local short-range spin arrangement implied by the checkerboard form for $S(\mathbf{Q})$ remains elusive. We know, however, that a simple FeF_3-type local noncollinear Néel structure, with tetrahedra corresponding to either all spins in or all spins out, fails to describe $S(\mathbf{Q})$.

Inelastic neutron measurements on both powders and single crystals reveal three bands of magnetic excitations, two of which are dispersionless at ~2.53 and 3.50 THz, and correspond to transitions between the ground-state doublet and singlet excited states. The low-lying band of excitations develops easily measurable dispersion below 20 K, and corresponds to a transition from the ground state to a doublet excited state. The nature of this dispersion is unclear, but the minima in energy occur at wave vectors for which $S(\mathbf{Q})$ is a relative maxima, even in the single crystals where $S(\mathbf{Q})$ is anisotropic. This dispersion vanishes at temperatures above which the mode is thermally occupied.

ACKNOWLEDGMENTS

It is a pleasure to acknowledge contributions from Z. Tun, I. Swainson, R. Donaberger, M. D. Lumsden, D. McK. Paul, F. Trouw, and C. V. Stager to these studies. We thank B. den Hertog, M. Gingras, M. Harris, and C. Kallin for many useful discussions. This research was funded by NSERC of Canada under the Collaborative Research Grant Geometrically Frustrated Magnetic Materials. This work has benefited from the use of the Intense Pulsed Neutron Source at Argonne National Laboratory. This facility was funded by the U.S. Department of Energy, BES-Materials Science, under Contract No. W-31-109-Eng-38. The work at Los Alamos was carried out under the auspices of the U.S. D.O.E.

*Present address: National Research Council, NPMR, Chalk River Laboratory, Chalk River, Ontario, Canada K0J 1J0.

†Present address: Department of Physics, Ohio State University, Columbus, Ohio 43210-1106.

[1] For recent reviews, see *Magnetic Systems with Competing Interactions*, edited by H. T. Diep (World Scientific, Singapore, 1994); A. P. Ramirez, Annu. Rev. Mater. Sci. **24**, 453 (1994); P. Schiffer and A. P. Ramirez, Comments Condens. Matter Phys. **18**, 21 (1996).

[2] G. H. Wannier, Phys. Rev. **79**, 357 (1950).

[3] M. A. Subramanian, G. Aravamudan, and G. V. Subba Rao, Prog. Solid State Chem. **15**, 55 (1983).

[4] P. W. Anderson, Phys. Rev. **102**, 1008 (1956).

[5] J. E. Greedan, J. N. Reimers, C. V. Stager, and S. L. Penny, Phys. Rev. B **43**, 5682 (1991).

[6] M. J. P. Gingras, C. V. Stager, N. P. Raju, B. D. Gaulin, and J. E. Greedan, Phys. Rev. Lett. **78**, 947 (1997).

[7] B. D. Gaulin, J. N. Reimers, T. E. Mason, J. E. Greedan, and Z. Tun, Phys. Rev. Lett. **69**, 3244 (1992).

[8] J. N. Reimers, J. E. Greedan, R. K. Kremer, E. Gmelin, and M. A. Subramanian, Phys. Rev. B **43**, 3387 (1991); a more recent publication by Y. Shimakawa, Y. Kubo, N. Hamada, J. D. Jorgensen, Z. Hu, S. Short, M. Nohara, and H. Takagi, *ibid.* **59**, 1249 (1999), suggests that $Y_2Mn_2O_7$ enters a ferromagnetic state below 15 K.

[9] M. J. Harris, M. P. Zinkin, Z. Tun, B. M. Wanklyn, and I. P. Swainson, Phys. Rev. Lett. **73**, 189 (1994).

[10] R. Moessner and J. T. Chalker, Phys. Rev. B **58**, 12 049 (1998).

[11] J. N. Reimers, Phys. Rev. B **45**, 7287 (1992).

[12] B. Canal and C. Lacroix, Phys. Rev. Lett. **80**, 2933 (1998).

[13] J. T. Chalker, P. C. W. Holdsworth, and E. F. Shender, Phys. Rev. Lett. **68**, 855 (1992).

[14] J. S. Gardner, B. D. Gaulin, and D. McK. Paul, J. Cryst. Growth **191**, 740 (1998).

[15] M. Kanada, Y. Yasui, M. Ito, H. Harashina, M. Sato, H. Okumura, and K. Kakurai, J. Phys. Soc. Jpn. **68**, 3802 (1999).

[16] M. J. P. Gingras, B. C. den Hertog, M. Faucher, J. S. Gardner, S. R. Dunsiger, L. J. Chang, B. D. Gaulin, N. P. Raju, and J. E. Greedan, Phys. Rev. B **62**, 6496 (2000).

[17] J. N. Reimers, J. E. Greedan, and M. Sato, J. Solid State Chem. **72**, 390 (1988).

[18] C. H. Booth, J. S. Gardner, G. H. Kwei, R. H. Heffner, F. Bridges, and M. A. Subramanian, Phys. Rev. B **62**, R755 (2000).

[19] J. S. Gardner, B. D. Gaulin, S.-H. Lee, C. Broholm, N. P. Raju, and J. E. Greedan, Phys. Rev. Lett. **83**, 211 (1999).

[20] M. J. Harris, S. T. Bramwell, T. Zeiske, D. F. McMorrow, and P. J. C. King, J. Magn. Magn. Mater. **177-181**, 757 (1998).

[21] M. P. Zinkin, M. J. Harris, Z. Tun, R. A. Cowley, and B. M. Wanklyn, J. Phys.: Condens. Matter **8**, 193 (1996).

[22] J. S. Gardner, S. R. Dunsiger, B. D. Gaulin, M. J. P. Gingras, J. E. Greedan, R. F. Kiefl, M. D. Lumsden, W. A. MacFarlane, N. P. Raju, J. E. Sonier, I. Swainson, and Z. Tun, Phys. Rev. Lett. **82**, 1012 (1999).

[23] M. J. Harris, S. T. Bramwell, D. F. McMorrow, T. Zeiske, and K. W. Godfrey, Phys. Rev. Lett. **79**, 2554 (1997).

[24] A. P. Ramirez, A. Hayashi, R. J. Cava, R. Siddharthan, and B. S. Shastry, Nature (London) **399**, 333 (1999); R. Siddharthan, B. S. Shastry, A. P. Ramirez, A. Hayashi, R. J. Cava, and S. Rosenkranz, Phys. Rev. Lett. **83**, 1854 (1999).

[25] Y. Shimakawa, Y. Kubo, and T. Manako, Nature (London) **379**, 53 (1996).

[26] J. W. Lynn, L. Vasiliu-Doloc, and M. A. Subramanian, Phys. Rev. Lett. **80**, 4582 (1998).

[27] S. H. Lee, C. Broholm, T. H. Kim, W. Ratcliff II, and S. W. Cheong, Phys. Rev. Lett. **84**, 3718 (2000).

[28] A. P. Ramirez, G. P. Espinosa, and A. S. Cooper, Phys. Rev. Lett. **64**, 2070 (1990).

[29] B. Martinez, A. Labarta, R. Rodrguez-Sol, and X. Obradors, Phys. Rev. B **50**, 15 779 (1994).

[30] C. Broholm, G. Aeppli, G. P. Espinosa, and A. S. Cooper, Phys. Rev. Lett. **65**, 3173 (1990).

[31] S. H. Lee, C. Broholm, G. Aeppli, T. G. Perring, B. Hessen, and A. Taylor, Phys. Rev. Lett. **76**, 4424 (1996).
[32] P. Schiffer, A. P. Ramirez, D. A. Huse, P. L. Gammel, U. Yaron, D. J. Bishop, and A. J. Valentino, Phys. Rev. Lett. **74**, 2379 (1995).
[33] J. A. Mydosh, Z. Phys. B: Condens. Matter **103**, 251 (1997).
[34] Byron C. den Hertog and M. J. P. Gingras, Phys. Rev. Lett. **84**, 3430 (2000).
[35] E. F. Bertaut and P. Burlet, Solid State Commun. **5**, 27 (1967).
[36] G. H. Lander, T. O. Brun, J. P. Desclaux, and A. J. Freeman, Phys. Rev. B **8**, 3237 (1973).
[37] G. Ferey, R. de Pape, M. LeBlanc, and J. Pannetier, Rev. Chim. Miner. **23**, 474 (1986).
[38] H. A. Mook, N. Wakabayashi, and D. Pan, Phys. Rev. Lett. **34**, 1029 (1975).
[39] See, for example, J. A. Blanco, R. M. Nicklow, and D. Schmitt, Phys. Rev. B **56**, 11 666 (1997).
[40] S. M. Shapiro, B. X. Wang, G. Shirane, J. Z. Larese, L. E. Tanner, and S. C. Moss, Physica B **156-157**, 59 (1989).
[41] R. P. Feynmann, in *Progress in Low Temperature Physics*, edited by C. Gorter (Interscience, New York, 1955), Vol. 1.
[42] P. Waldron, M.Sc. thesis, McMaster University, Canada, 2000.